F. Carpignano, G. Rigamonti, S. Merlo, **Characterization of rectangular glass micro-capillaries by low-coherence reflectometry**, *IEEE Photonics Technology Letters*, Vol. 27, No. 10, May 15, 2015, pp. 1064-1067, Piscataway, NJ, USA (2015). DOI: 10.1109/LPT.2015.2407271

Characterization of rectangular glass micro-capillaries by low-coherence reflectometry

Francesca Carpignano, Giulia Rigamonti, and Sabina Merlo, *Senior Member, IEEE*

***Abstract*—We report the functionality of optical low-coherence reflectometry (OLCR) to characterize glass micro-capillaries with 50-µm-deep rectangular cross-section, in view of their application as micro-opto-fluidic devices. We exploited infrared radiation generated by a Tungsten lamp in a time-domain low-coherence interferometer based on a fiberoptic Michelson scheme. OLCR allowed us to easily detect the optical distance between in-depth interfaces of the capillary as well as the refractive index of ethylene glycol solutions in water at different concentrations, which were inserted into the channel by capillary action.**

***Index Terms*—Optical low-coherence reflectometry, Distance measurements, Glass rectangular micro-capillary, Infrared radiation, Refractive index measurements.**

I. Introduction

Optical low-coherence reflectometry (OLCR) is an interesting diagnostic tool for characterizing optical components [1]–[8]. It is a very powerful technique that enables detection of the relative position of interfaces due to refractive index changes in the device under test. Briefly, if broadband radiation is launched into a Michelson interferometer, groups of fringes are developed only when the time delays of the two arms are equal. In time-domain OLCR a mirror of the Michelson scheme is replaced by the device with internal interfaces that back-reflect light: as the mirror on the reference arm is displaced, fringes are detected when the time delay to the mirror matches the delay to a reflection site within the tested device.

Recently, OLCR schemes in the frequency domain were developed in order to replace the mirror mechanical scanning with the analyses of the interference spectrum [3], [4], [9]. Basically, these solutions require a combination of a broadband light source with a spectrometer or a swept source with a photodetector. In these cases, complex optoelectronic instrumentation as well as signal processing is needed. Such advanced solutions are mainly justified by the request of rapidly forming 3D images of the material or device under test, such as in optical coherence tomography. On the other hand, spot optical measurements can be sufficient for diagnostic or sensing purposes. In particular, non-contact techniques for in-depth non-destructive characterization of multilayered microstructures are becoming necessary in order to detect the layer thickness and the optical distance between interfaces.

Recently, low-cost rectangular glass capillaries were successfully proposed as resonators for non-contact trapping using acoustic standing waves [10], [11]. Other investigators previously exploited similar devices for capillary zone electrophoresis to obtain high-resolution separations in the analysis of complex mixtures [12]. These applications require a good matching between the channel dimensions and the applied operational frequency. Moreover, rectangular capillaries would be of great interest also in other micro-opto-fluidic systems where optical imaging or spot measurements need to be performed.

In this letter, we are reporting the application of a time-domain optical low-coherence reflectometer based on a compact fiberoptic (FO) configuration to characterize glass micro-capillaries with 50-µm-deep, rectangular cross-section. The implemented configuration exploits infrared (IR) broadband radiation, generated by a fiber-coupled Tungsten lamp in the wavelength range of 1.2 µm to 1.7 µm, to ensure a longitudinal resolution better than 2 µm. Similar performances in the IR were previously demonstrated by other authors with more expensive and complex light sources or with free-space optical setups [5], [13]–[17]. With our configuration for OLCR, the optical path lengths of the glass walls and of the inner channel were detected by shining radiation perpendicularly to the flat surfaces of the capillary under test. Fluid samples (water-ethylene glycol solutions at different concentrations) were easily collected by capillary action without affecting the channel size. Therefore, the optical path changes measured by OLCR were directly related to the refractive index of the tested solution. We foresee application of rectangular glass capillaries as micro-cuvettes for biochemical analyses based on optical readout techniques.

II. Instrumental Configuration

The optical and instrumental configuration realized for IR OLCR is shown in Fig. 1. In our scheme, based on an all-fiber Michelson interferometer, two bidirectional 2x2 FO couplers with 50:50 splitting ratio and flat spectral response were

Manuscript received December 31, 2014; revised January 26, 2015. This work was partially funded by Fondazione CARIPLO, Grant no. 2011-0308.

F. Carpignano, G. Rigamonti and S. Merlo are with Dipartimento di Ingegneria Industriale e dell'Informazione, Università degli Studi di Pavia, 27100 Pavia, Italy (e-mail: carpignano@unipv.it, giulia.rigamonti01@universitadipavia.it, merlo@ieee.org).

Color versions of the figures in this paper are available online at http://ieeexplore.ieee.org.

Digital Object Identifier 10.1109/LPT.2015…..

employed. Interferometric signal detection was performed by means of a balanced receiver [18]. Broadband radiation, after crossing the first FO splitter, was launched into the second coupler, which redirected part of the radiation along the "measuring arm" toward the capillary and part of the radiation along the "reference arm" toward the reference mirror. Radiation reflected by the mirror and by the various interfaces within the capillary was coupled back into the fibers and carried toward the InGaAs photodiodes (PhD1 and PhD2 in Fig. 1). They were incorporated into a custom-designed balanced receiver that enabled efficient detection of the interferogram (*i.e.*, the interferometric fringes) by removing the DC component as well as other common mode signal components [18]. Electronic amplification of the photogenerated signals was regulated in order to compensate for the different optical power reaching the photodiodes. The output voltage of the balanced receiver was connected to an analog to digital (A/D) conversion board for easy signal acquisition with a personal computer (PC).

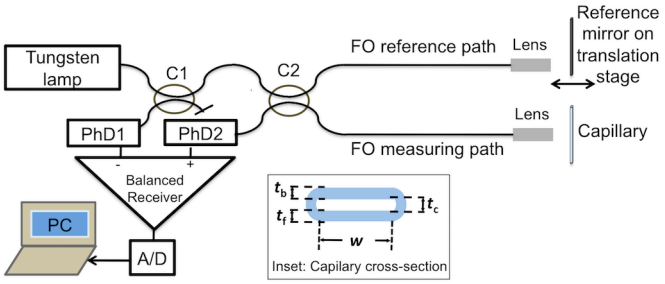

Fig. 1. Instrumental and optical configuration for low-coherence infrared reflectometer. PhD: InGaAs photodiode. A/D: analog to digital conversion board. PC: personal computer. FO: fiberoptic. C: bidirectional 2x2 FO couplers with 50:50 splitting ratio and flat spectral response. Inset: schema of the capillary cross-section. t_f, t_b: thickness of the front and back glass wall. t_c: depth of the inner channel. w: width of the flat side of the capillary.

Readout radiation was provided by a Tungsten lamp with an emitted power spectral density (coupled in SMF) of about -60 dBm/10 nm in the wavelength range from 1.2 µm to 1.7 µm. Both interferometer arms incorporated the same fiber paths, matched in length within 1 mm, whereas the final sections were in open space; we used matched fiberoptic patch-cords and optical components in both interferometer arms to minimize the difference in optical dispersion and exploit the high axial resolution (better than 2 µm) offered by the intrinsic short coherence length of the source. At the end of both arms, pigtail-style focusers with aspheric lens were used as readout lenses, generating a 50-µm-diameter spot at the working distance of 23.5 mm. The fiber components were all based on standard telecommunication optical fibers (9/125 µm core/cladding diameter Single Mode Fiber, SMF). A computer-controlled, motorized translation stage allowed to move the reference mirror (at velocity v = 5 µm/s) in order to change the length of the reference path.

Several experiments were performed and repeated in different days and months also with different broadband sources without observing substantial variations of the results in terms of interferometric signals in the time domain.

Optical measurements were performed at room temperature in a laboratory environment, without the use of a feedback loop for thermal monitoring/control on the interrogated volume; limitations in the measurement accuracy were attributed to local temperature variations.

III. Experimental Results

We applied IR OLCR for characterizing borosilicate glass capillaries with rectangular-section channel, also known as rectangle hollow capillary tubes (Vitrotubes™, VitroCom, New Jersey, USA). The thickness t_f and t_b of the front and back glass wall, respectively, as well as the depth t_c of the inner channel were nominally equal to 50 µm whereas the width (w) of the flat side was w = 500 µm (see capillary cross-section in the inset of Fig. 1). The capillaries were 50-mm-long. Standard tolerances of inner dimensions are of +/-10%.

The interferometric signal was acquired in the time domain and the travelling time T was then easily converted into optical path (OP) using the stage velocity v, *i.e.*, $OP = v \cdot T$. Using a broadband light source, we obtained a narrowband photodetected signal; thus a digital band-pass filter was very effective for improving the signal-to-noise ratio.

A typical interferometric signal, digitally filtered and normalized with respect to the peak value, collected on an empty 50-µm capillary is shown in Fig. 2.

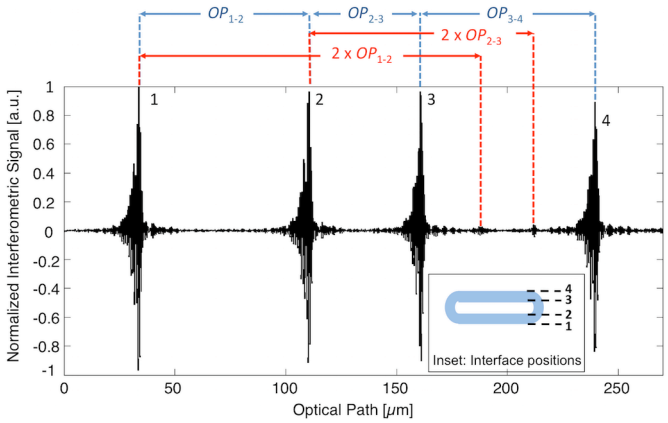

Fig. 2. Normalized interferometric signal as a function of the optical path obtained on an empty 50-µm capillary. OP_{1-2}, OP_{2-3} OP_{3-4}: optical path relative to the front glass wall, to the channel, and to the back glass wall, respectively. 2xOP_{1-2}, 2xOP_{2-3}: double round-trip in the front glass wall and in the channel. 1, 2, 3 and 4: Interface positions, as shown in the inset.

Four groups of fringes with approximately unitary amplitude are easily recognized. They correspond to the air-glass interfaces crossed by the readout radiation. Two additional groups of fringes with much lower amplitude are present between the 3rd and 4th large peaks. One is due to a double round-trip in the front glass wall and the other to a double round-trip in the channel. We then applied the Hilbert transform [19], [20] to obtain the envelope of the interferometric signals and identify more easily the peak positions. In fact, envelope conversion by means of Hilbert transformation usually improves the resolution of the measurements since it reduces the noise of the interferogram, increase data density and provides smaller measuring steps [21].

Fig. 3 shows the envelope (black trace) of the interferometric signal reported in Fig. 2: the effective channel depth was obtained as the optical distance $OP_{2\text{-}3}$ between the 2nd and the 3rd group of unitary amplitude fringes and for this capillary sample we found $OP_{2\text{-}3,air}$ = 50.61 ± 0.01 µm, thus in agreement with the fabrication tolerances. The optical paths relative to the front and back glass walls were $OP_{1\text{-}2}$ = 76.46 ± 0.05 µm and $OP_{3\text{-}4}$ = 78.61 ± 0.16 µm, respectively. Mean values and standard deviations were always calculated at least on three data sets.

As it is well-known, the optical path distance OP, in the case of broadband radiation and dispersive media, is given by $OP = n_g \cdot t$, where n_g is the group refractive index (RI) of the medium crossed by radiation and t the material thickness [2]. Assuming for the group refractive index of borosilicate glass $n_{g,glass} \approx 1.52$ RIU [15] (for wavelengths in the range from 1.55 µm up to 1.58 µm), we obtained for this capillary sample the following values of glass thickness: $t_f = OP_{1\text{-}2} / n_{g,glass}$ = 50.30 µm and $t_b = OP_{3\text{-}4} / n_{g,glass}$ = 51.72 µm, as expected for this capillary size.

Fig. 3 shows also the envelope of the interferometric signal acquired after filling the capillary channel with water (red trace). An interesting feature of these devices is that the liquid sample is collected instantly from a vial by capillary action. Moreover, the fluid does not affect the channel size. As expected, the optical path between the 1st and 2nd group of fringes did not change, whereas an increase of the optical path between the 2nd and 3rd was clearly observed in presence of water. Moreover, the amplitude of the 2nd and 3rd group of fringes was smaller than that of the 1st and 4th group. This result is in agreement with the fact that the index difference between water and glass is lower than that between air and glass.

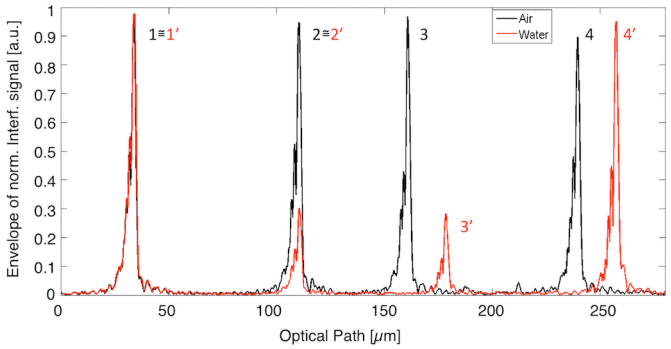

Fig. 3. Envelope of the normalized interferometric signal obtained with Hilbert transform as a function of the optical path for a 50-µm capillary. Black trace: empty capillary; red trace: capillary filled with water. 1, 2, 3 and 4: Interfaces for empty capillary; 1', 2', 3'and 4': Interfaces for capillary filled with water.

The experimental value of the group RI of water was then obtained as $n_{g,water} = OP_{2\text{-}3,water}/OP_{2\text{-}3,air} = OP_{2\text{-}3,water}/t_c$ = 1.341 RIU. This result is in agreement with the group RI of water ($n_{g\text{-}th,water}$=1.349 RIU) calculated for wavelengths in the range from 1.55 µm up to 1.58 µm with the relation $n_g = n_f - \lambda \cdot (dn/d\lambda)$, where n_f is the phase refractive index, λ is the center wavelength and $dn/d\lambda$ is the chromatic dispersion, and the values at 25 °C of n_f and $dn/d\lambda$ reported in the literature [22].

We confirmed the result $n_{g,water}$= 1.341±0.001 RIU in several experiments, performed on different capillary samples, since water represented the reference fluid of various tested mixtures.

We then applied OLCR for testing the rectangular capillary filled with solution of ethylene glycol (EG) in water (H_2O) at different concentrations. For each fluid sample, from the acquired interferometric signal we extracted the optical paths relative to the glass walls and to the channel. These data are reported in Fig. 4 as functions of EG concentration expressed in %. As expected, $OP_{1\text{-}2}$ and $OP_{3\text{-}4}$ did not show any dependence on the solution type. On the other hand, a linear increase of the optical path $OP_{2\text{-}3}$ relative to the channel was found by augmenting EG concentration.

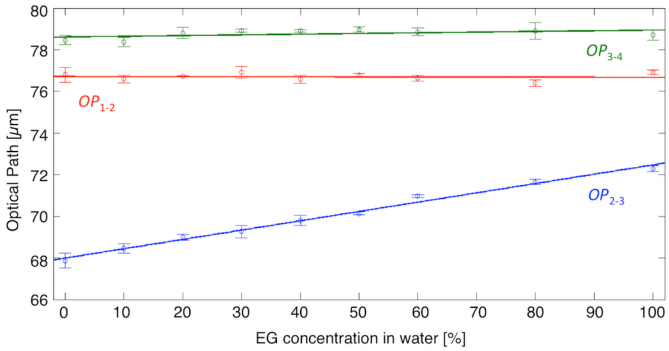

Fig. 4. Optical paths (OP) relative to the glass walls and to the channel as functions of the ethylene glycol (EG) concentration in water expressed in % for a 50-µm capillary. Blue markers: $OP_{2\text{-}3}$ (optical path of the inner channel); red markers: $OP_{1\text{-}2}$; green markers: $OP_{3\text{-}4}$. Lines: linear best fitting of data.

Finally, we calculated the group refractive indexes of the various EG-H_2O solutions (dividing the experimental values of $OP_{2\text{-}3}$ by $OP_{2\text{-}3,air}$) and we report them as a function of EG concentration in Fig. 5 (red circles).

Although the relationship between n_g and n_f is in principle non-linear, if we consider refractive index variations in a small range a linear approximation yields sufficiently accurate results. In view of this observation, we also show for comparison in Fig. 5 the values found in the literature for phase RI (blue dots) at $\lambda \approx 0.589$ µm of EG-H_2O solutions [23].

It is interesting to note that by linear best fitting the RI data relative to EG concentrations (C) from 0% up to 60%, we obtained a refractive index increment $dRI/dC \approx 1 \cdot 10^{-3}$ [RIU/%EG] for both ensembles of data.

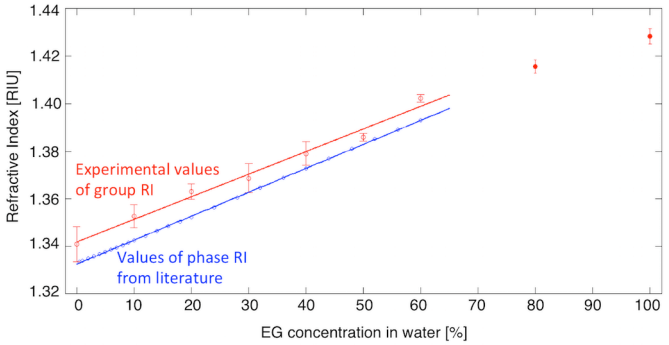

Fig. 5. Refractive index of EG-H_2O solutions as a function of the EG concentration. Red circles with error bars: experimental values of group RI measured by OLCR; red line: linear best fitting of the experimental data from 0% up to 60% of EG in water; blue markers: phase RI from ref. [23]; blue line: linear best fitting of literature data.

IV. Conclusions

We have demonstrated the functionality of an all-fiber infrared low-coherence reflectometer for detecting the optical distance between the interfaces of a rectangular capillary with micrometric dimension, also in presence of fluids in the channel. Since the depth of the inner channel is fixed, the group refractive index of the collected sample fluid can be obtained. Method accuracy was demonstrated by measuring the group refractive index of water that was found in accordance with literature data specific for the near infrared. Moreover, the accuracy is adequate for characterizing off-the-shelf glass micro-capillaries, as the measured geometrical parameters are in agreement with the nominal size and well within the fabrication tolerances. Indeed, glass micro-capillaries represent an interesting solution for the implementation of low-cost devices for (bio)sensing since they could be easily integrated in micro-fluidic system, allowing repeatable and fast measurements. For biosensing applications, currently under investigation, the Tungsten lamp features in addition to the high axial resolution the further advantage of minimum invasiveness on the biological sample thanks to the very low optical power density and the specific wavelength range. Our setup benefits also of the use of active and passive optical components suitable for the infrared spectral region that are commercially available and already well developed for optical communications.

Acknowledgment

The authors wish to thank G. Barillaro, G. Mazzini, G. Silva, and S. Surdo for fruitful discussions.

References

[1] R. C. Youngquist, S. Carr, and D. E. N. Davies, "Optical coherence-domain reflectometry: a new optical evaluation technique," *Opt. Lett.*, vol. 12, no. 3, pp. 158–160, 1987.

[2] W. V. Sorin and D. F. Gray, "Simultaneous thickness and group index measurement using optical low-coherence reflectometry," *IEEE Photonics Technol. Lett.*, vol. 4, no. 1, pp. 105–107, 1992.

[3] B. H. Lee, E. J. Min, and Y. H. Kim, "Fiber-based optical coherence tomography for biomedical imaging, sensing, and precision measurements," *Opt. Fiber Technol.*, vol. 19, no. 6, pp. 729–740, 2013.

[4] J. Izatt and M. Choma, "Theory of Optical Coherence Tomography," in *Optical Coherence Tomography*, W. Drexler and J. G. Fujimoto, Eds. Springer, 2008, pp. 47–72.

[5] L. Vabre, A. Dubois, and A. C. Boccara, "Thermal-light full-field optical coherence tomography," *Opt. Lett.*, vol. 27, no. 7, pp. 530–532, 2002.

[6] S. Combrié, N. V. Q. Tran, E. Weidner, A. De Rossi, S. Cassette, P. Hamel, Y. Jaouën, R. Gabet, and A. Talneau, "Investigation of group delay, loss, and disorder in a photonic crystal waveguide by low-coherence reflectometry," *Appl. Phys. Lett.*, vol. 90, no. 23, p. 231104, 2007.

[7] A. Parini, P. Hamel, A. De Rossi, S. Combrié, N. Tran, Y. Gottesman, R. Gabet, A. Talneau, Y. Jaouën, and G. Vadalà, "Time-wavelength reflectance maps of photonic crystal waveguides: a new view on disorder-induced scattering," *J. Light. Technol.*, vol. 26, no. 23, pp. 3794–3802, 2008.

[8] R. Gabet, P. Hamel, Y. Jaouën, A. Obaton, V. Lanticq, and G. Debarge, "Versatile characterization of specialty fibers using the phase-sensitive optical low-coherence reflectometry technique," *J. Light. Technol.*, vol. 27, no. 15, pp. 3021–3033, 2009.

[9] I. K. Ilev, S. A. Boppart, S. Andersson-Engels, B. M. Kim, L. Perelman, and V. Tuchin, "Issue on Biophotonics," *IEEE J. Sel. Top. Quantum Electron.*, vol. 20, no. 2, p. 0200204, 2014.

[10] B. Hammarström, M. Evander, H. Barbeau, M. Bruzelius, J. Larsson, T. Laurell, and J. Nilsson, "Non-contact acoustic cell trapping in disposable glass capillaries.," *Lab Chip*, vol. 10, no. 17, pp. 2251–2257, 2010.

[11] M. Evander and M. Tenje, "Microfluidic PMMA interfaces for rectangular glass capillaries," *J. Micromechanics Microengineering*, vol. 24, no. 2, p. 027003, 2014.

[12] T. Tsuda, J. V. Sweedler, and R. N. Zare, "Rectangular capillaries for capillary zone electrophoresis," *Anal. Chem.*, vol. 62, no. 19, pp. 2149–2152, 1990.

[13] Y. Wang, Y. Zhao, J. S. Nelson, Z. Chen, and R. S. Windeler, "Ultrahigh-resolution optical coherence tomography by broadband continuum generation from a photonic crystal fiber," *Opt. Lett.*, vol. 28, no. 3, pp. 182–4, 2003.

[14] M. Ohmi and M. Haruna, "Ultra-high resolution optical coherence tomography (OCT) using a halogen lamp as the light source," *Opt. Rev.*, vol. 10, no. 5, pp. 478–481, 2003.

[15] P. Cimalla, J. Walther, M. Mehner, M. Cuevas, and E. Koch, "Simultaneous dual-band optical coherence tomography in the spectral domain for high resolution in vivo imaging," *Opt. Express*, vol. 17, no. 22, pp. 19486–19500, 2009.

[16] Y. Chen, H. Zhao, and Z. Wang, "Investigation on spectral-domain optical coherence tomography using a tungsten halogen lamp as light source," *Opt. Rev.*, vol. 16, no. 1, pp. 26–29, 2009.

[17] J. Xu, H. Ou, X. Wang, P. C. Chui, H. Y. Tam, and K. K. Y. Wong, "In vivo OCT imaging based on la-codoped bismuth-based erbium-doped Fiber," *IEEE Photonics Technol. Lett.*, vol. 25, no. 17, pp. 1741–1743, 2013.

[18] A. M. Rollins and J. A. Izatt, "Optimal interferometer designs for optical coherence tomography," *Opt. Lett.*, vol. 24, no. 21, pp. 1484–1486, 1999.

[19] K. G. Larkin, "Efficient nonlinear algorithm for envelope detection in white light interferometry," *J. Opt. Soc. Am. A*, vol. 13, no. 4, pp. 832–843, 1996.

[20] P. Pavliček and V. Michálek, "White-light interferometry—envelope detection by Hilbert transform and influence of noise," *Opt. Lasers Eng.*, vol. 50, no. 8, pp. 1063–1068, 2012.

[21] Y. Watanabe and I. Yamaguchi, "Digital Hilbert transformation for separation measurement of thicknesses and refractive indices of layered objects by use of a wavelength-scanning heterodyne interference confocal microscope," *Appl. Opt.*, vol. 41, no. 22, pp. 4497–4502, 2002.

[22] "SOPRA N&K database." [Online]. Available: http://refractiveindex.info.

[23] D. R. Lide, "Physical Constants of Organic Compounds," in *CRC Handbook of Chemistry and Physics*, CRC Press, Ed. Boca Raton, 2005, p. 8—63.